Journal of Hazardous Materials 414 (2021) 125552

Contents lists available at ScienceDirect

Journal of Hazardous Materials

journal homepage: www.elsevier.com/locate/jhazmat

Research Paper

Oily sludge derived carbons as peroxymonosulfate activators for removing aqueous organic pollutants: Performances and the key role of carbonyl groups in electron-transfer mechanism

Wenjie Liu [a,1], Chunyang Nie [a,1], Wenlang Li [a], Zhimin Ao [a,*], Shaobin Wang [b], Taicheng An [a]

[a] *Guangzhou Key Laboratory of Environmental Catalysis and Pollution Control, Guangdong Key Laboratory of Environmental Catalysis and Health Risk Control, Institute of Environmental Health and Pollution Control, School of Environmental Science and Engineering, Guangdong University of Technology, Guangzhou 51006, China*

[b] *School of Chemical Engineering and Advanced Materials, University of Adelaide, Adelaide SA 5005, Australia*

ARTICLE INFO

Editor: Dr. B. Lee

Keywords:
Carbocatalyst
PMS
Hazardous waste
Electron-transfer oxidation
Recalcitrant pollutants

ABSTRACT

In this work, low-cost carbon-based materials were developed via a facile one-pot pyrolysis of oily sludge (OS) and used as catalysts to activate peroxymonosulfate (PMS) for removing aqueous recalcitrant pollutants. By adjusting the pyrolysis temperature, the optimized OS-derived carbocatalyst manifested good performance for PMS activation to abate diverse organic pollutants in water treatment. Particularly, an average removal rate of 0.87 mol phenol per mol PMS per hour at a catalyst dosage of 0.2 g L^{-1} is attained by the OS-derived carbocatalyst, higher than many other documented catalysts. A series of experimental evidences consolidated that organic pollutants were oxidized mainly via electron-transfer mechanism albeit the detection of singlet oxygen ($^1O_2$) from PMS activation driven by the OS-derived carbocatalyst. Specifically, the proportion of carbonyl groups (C=O) in the carbocatalyst adopted with selective modification treatments to tailor the surface chemistry was found to be linearly correlated with the catalytic activity and theoretical calculations demonstrated that the reactions between C=O and PMS to form surface reactive complexes were more energetically favorable compared to $^1O_2$ generation. Herein, this study not only offers a new strategy for reusing OS as value-added persulfate activators but also deepens the fundamental understanding on the nonradical regime.

1. Introduction

In the past few decades, persulfate-based advanced oxidation processes (PS-AOPs), which reactive oxygen species (ROS) including free radicals and non-free radicals are generated from persulfate (peroxymonosulfate (PMS) and peroxydisulfate (PDS)) activation, have been demonstrated to be effective techniques for eliminating refractory organics in contaminated water (Sun et al., 2014; Duan et al., 2015, 2018b; Ma et al., 2019). Because of the good performance, biocompatibility, and sustainability, carbon-based materials (nanocarbons and biochar) have recently emerged as promising alternatives to the traditional metal-based catalysts as persulfate activators (Indrawirawan et al., 2015; Lee et al., 2015; Duan et al., 2016, 2018a; Guan et al., 2016; Wang et al., 2016; Ghanbari and Moradi, 2017; Ike et al., 2018; Ren et al., 2019; Nie et al., 2019; Meng et al., 2020; Nie et al., 2020). Compared to nanocarbons, biochar deriving from the ubiquitous agricultural wastes and sewage sludge shows merits of low cost, facile synthesis and high catalytic activity, which enable promising practicability in PS-AOPs (Mian et al., 2019). Apart from agricultural wastes and sewage sludge, other types of industrial wastes can also serve as promising precursors to fabricate high-performance carbocatalysts via simple synthetic procedures, which has been paid little attention.

Oily sludge (OS) accumulated from the petroleum industry is classified as a hazardous waste because it is characterized as an emulsion of water, petroleum hydrocarbons, solid particles and heavy metals (Yuan et al., 2018). More than 60 million tons of OS can be produced yearly around the world (Hu et al., 2013). Thereby, proper treatment processes on OS to minimize its potential threats to the environment and human health are of great significance. A variety of methods have been developed for the treatment of oily sludge, including advanced oxidation (Ferrarese et al., 2008), biodegradation (Kriipsalu et al., 2007; Fernandez-Luqueno et al., 2011; Ma et al., 2014; Nazem and Tavakoli,

---

[*] Corresponding author.
E-mail address: zhimin.ao@gdut.edu.cn (Z. Ao).

[1] These authors contributed equally to this work.

https://doi.org/10.1016/j.jhazmat.2021.125552
Received 8 January 2021; Received in revised form 20 February 2021; Accepted 23 February 2021

2017), incineration (Malviya and Chaudhary, 2006), stabilization/solidification (Malviya and Chaudhary, 2006), solvent extraction (Paranhos Gazineu et al., 2005; Ávila-Chávez et al., 2007; Zubaidy and Abouelnasr, 2010), centrifugation (Nii et al., 2009), freezing/thawing therapy (Lai et al., 2004), pyrolysis (Pánek et al., 2014; Wang et al., 2017) and so on (as summarized in Table S1). Among these methods, pyrolysis is the most popular one because it is easy-handled and does not need expensive chemicals or complex equipment. Particularly, not only the hydrocarbons can be recycled from OS into fuel for reuse through the pyrolysis treatment, but also the resultant solid products (called as char) can be applied as adsorbents for gaseous pollutants like H_2S or NO_X (Fonts et al., 2012), carbon electrode materials (Meng et al., 2016), etc. due to the porous and carbon-rich feature of char. In this regard, OS can also be used as a proper precursor to prepare carbon-based catalysts via pyrolysis for activating persulfate, which offers a new value-added approach for the reuse of OS. Unfortunately, since the previous studies for pyrolysis of oily sludge mainly focused on recycling products such as hydrocarbons and non-condensable gases, the application of OS-derived carbonaceous materials (char) in PS-AOPs has barely been reported.

At the initial stage of research on carbon-driven persulfate activation, free radicals such as sulfate radical ($SO_4^{\bullet-}$) and hydroxyl radical (•OH) with high oxidative potential were found to be the main generated ROS (Lei et al., 2019; Li et al., 2019; Zhang et al., 2019). As more researches progressed, nonradical oxidation pathways were widely discovered in various carbocatalyst/persulfate systems (Cheng et al., 2016; Yun et al., 2018; Luo et al., 2019; Nie et al., 2019; Meng et al., 2020; Nie et al., 2020). Compared to the radical-based oxidation processes, nonradical oxidation pathways manifest several advantages including the better selectivity towards organic pollutants, less production of toxic byproducts from the oxidation of halide ions, minimized persulfate consumption, etc. (Duan et al., 2018b, 2019; Yun et al., 2018; Nie et al., 2019; Li et al., 2020) thus attracting more attention from the scientific community.

Singlet oxygenation and mediated electron transfer oxidation (persulfate is bounded onto the carbocatalyst to form surface reactive complexes for oxidizing organics) are two mainstream nonradical oxidation pathways (Duan et al., 2018a, 2018c). However, there are still several uncertainties for the two pathways, like the experimentally accurate identification of the oxidation pathway and evolution processes of nonradical reactive species. Singlet oxygen ($^1O_2$) is considered as the primary ROS dominating the nonradical oxidation of organic pollutants based on quenching tests and electron paramagnetic resonance (EPR) detection using 2,2,6,6-tetramethylpiperidine (TEMP) as a spin-trapping agent (Meng et al., 2020), while the electron-transfer mechanism is identified by excluding the generation of $^1O_2$ (Zhou et al., 2015, 2017). However, identifying singlet oxygenation mechanism based on quenching tests is not very reliable because the commonly used $^1O_2$ quenchers like azide and L-histidine themselves can deplete persulfate to cause an inhibitory effect on the organics degradation (Yun et al., 2018). Especially, a few recent works have carried out in-depth investigations and demonstrated that, although $^1O_2$ was detected by EPR in nonradical carbocatalyst/persufate systems, electron-transfer mechanism was responsible for the degradation of organics through various experimental evidences (Yun et al., 2018; Wang et al., 2019). Therefore, it should be prudent to experimentally determine the nonradical pathway between singlet oxygenation and mediated electron transfer process.

To understand the evolution processes of nonradical reactive species, it is essential to accurately determine the active sites on carbocatalysts. Carbonyl groups (C=O), as a Lewis basic site on carbocatalysts, have been demonstrated to show the highest catalytic reactivity towards persulfate activation among various oxygen groups from both theoretical and experimental aspects (Wang et al., 2016; Sun et al., 2017). Particularly, the C=O on carbocatalysts has been postulated to play a critical role in the singlet oxygenation mechanism since ketones were reported to accelerate the $^1O_2$ generation associated with persulfate decomposition (Brauer et al., 2002; Zhou et al., 2015; Yun et al., 2018; Sun et al., 2020). However, as a result of the controversy in identifying the nonradical pathways, the role of C=O on carbocatalysts in activating persulfate to form $^1O_2$ remains to be clarified. Notably, several recent studies proposed that defects or electron-deficient C atoms on a carbocatalyst were responsible for the $^1O_2$ generation (Cheng et al., 2019; Sun et al., 2020). Hence, more efforts on exploring the role of C=O on carbocatalysts in nonradical persulfate activation and the intrinsic catalytic mechanisms are of necessity, which are crucial to the fundamental understanding of the nonradical regime in PS-AOPs.

Herein, OS wastes were utilized as precursors to prepare carbon-based catalysts at different temperatures and their catalytic performances for PMS activation and oxidative degradation of organic micropollutants were evaluated. The OS-derived carbocatalyst prepared at 600 °C was found to exhibit the best performance and it served as a cost-effective PMS activator for abating phenolics, halogenated compound and antibiotics. Meanwhile, an electron-transfer oxidation mechanism responsible for the PMS activation over OS-derived carbons was identified by a thorough investigation, including radical screening tests, EPR, solvent exchange, and competitive organics degradation. More importantly, the role of C=O on the OS-derived carbocatalyst in nonradical persulfate activation processes ($^1O_2$ vs. electron-transfer) was clarified by combining experimental results (investigating the relationship between surface density of C=O and PMS activation efficiency) with computational calculations (comparing the thermodynamics of reactions between C=O and PMS for forming surface reactive complexes with that for forming $^1O_2$). Based on these results, we hope to not only provide an important technical support for the proper disposal and reuse of OS wastes in water remediation, but also highlight the key role of C=O on a carbocatalyst in electron-transfer mechanism, which deeps the understanding of the non-radical mechanism in carbon-based AOPs.

2. Materials and methods

2.1. Materials

PMS ($2KHSO_5 \cdot KHSO_4 \cdot K_2SO_4$) was supplied by Alfa Assar. PDS was provided by Acros Organics. Hydrochloric acid (HCl), nitric acid (HNO_3) and sodium hydroxide (NaOH) were purchased from Guangzhou Chemical Reagent Factory (China). Hydrazine hydrate (N_2H_4) was purchased from Tianjing Chemical Reagent Factory (China). Ethanol was purchased from Fisher Chemical. Methanol of a chromatographic grade was supplied by ANPEL Laboratory Technologies (Shanghai) Inc. 5,5-dimethyl-1-pyrroline-n-oxide (DMPO) was purchased from Sigma-Aldrich while TEMP was purchased from J&K Scientific. Bisphenol A (BPA) was provided by Tokyo Kasei Kogyo (Tokyo, Japan). Carbamazepine, 2,4-dichlorobromobenzene, phenol, furfuryl alcohol (FFA) and heavy water (D_2O) were provided by Aladdin (Shanghai, China). All the chemicals were of analytical grade and were used without further purification. Ultrapure water of 18.2 MΩ was employed to prepare all solutions.

2.2. Synthesis of catalysts

OS obtained by flocculated organic materials from oily wastewater was provided by Sinopec Maoming Branch. The pristine OS was heated in an oven at 80 °C for dewatering. Then, the dried OS loaded in a ceramic crucible was transferred to a tubular furnace and heated to designated temperature at a heating rate of 5 °C min^{-1} for 6 h under a nitrogen flow. The resultant carbon-based catalysts were denoted as OS-X, where X represents the pyrolysis temperature. To remove the residual metal impurities, the OS-X samples were dispersed into 200 mL HCl solution (0.1 M) and stirred for 2 h. Subsequently, the suspension was filtered and washed repeatedly with ultrapure water until the pH of filtrate was neutral. Finally, the washed samples were dried at 70 °C for 24 h and the obtained dry powders were denoted as OS-X-AW.

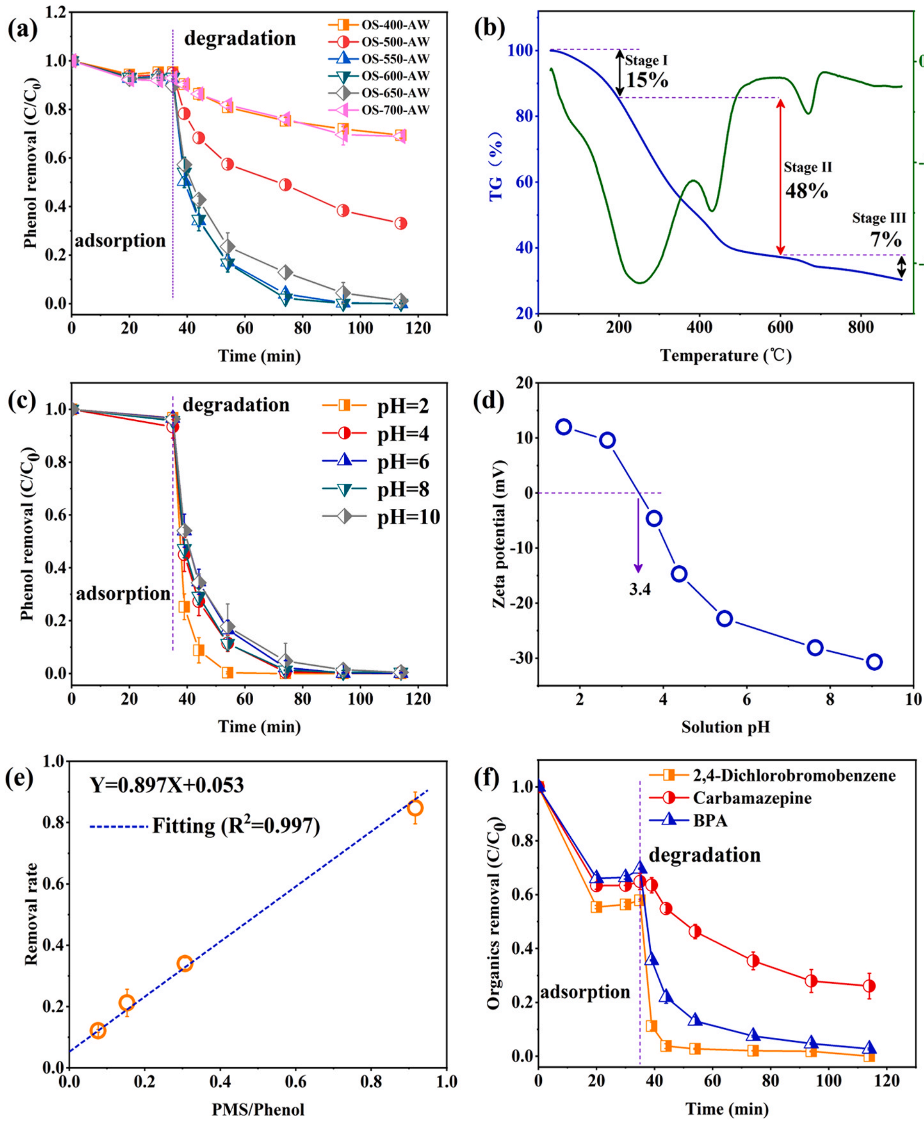

Fig. 1. (a) Phenol removals by different OS-X-AW/PMS systems; (b) TG and DTG curves of OS; (c) Effect of initial pH on phenol removal by OS-600-AW/PMS system; (d) Zeta potential as a function of pH for OS-600-AW; (e) the fitting curve of phenol removal rate versus [PMS]/[phenol] ratio; (f) Organics removal in the OS-600-AW/PMS system. Conditions: [catalyst] = 0.2 g L^{-1}, [2,4-Dichlorobromobenzene]$_0$ = [BPA]$_0$ = [phenol]$_0$ = 50 mg L^{-1}, [Carbamazepine]$_0$ = 20 mg L^{-1}, [PMS]$_0$ = 0.925 mM.

OS-600-AW was combusted in a tubular furnace with air convection at 1000 °C with a heating rate of 5 °C min^{-1} for 10 min and the obtained solid residue was denoted as e-OS-600-AW. Chemical oxidation and reduction treatments on OS-600-AW were performed using 3.1 M HNO_3 or H_2SO_4 solution and 3.1 M N_2H_4 solution at 70 °C for 4 h, separately. The derived samples were washed with deionized water until neutral pH was reached. Then the samples were dried in an oven at 70 °C for 24 h before usage.

2.3. *Experimental procedures of pollutant degradation*

Phenol, BPA, 2,4-dichlorobromobenzene and carbamazepine were selected as the model pollutants to assess the catalytic activity of the as-prepared catalysts for PMS activation. The micropollutants degradation experiments were conducted in conical flasks at room temperature. First, a certain amount of the as-prepared samples were vigorously mixed with 50 ppm phenol solution in a conical flask under magnetic stirring for 35 min to establish the adsorption-desorption equilibrium of organics onto the catalysts. Then a certain amount of PMS was added into the mixture to initiate the activation process. At the predetermined time interval, a certain amount of aliquot was sampled from the reaction suspension and then transferred into a high-performance liquid chromatography (HPLC) vial rapidly through a syringe filter with polyether sulfone membrane of 0.22 μm. All the degradation experiments were conducted in duplicate or triplicate, and the mean and its standard deviations were presented.

2.4. *Analytical methods*

The concentrations of organic pollutants were measured using HPLC (Elite EC1assical3100) with a C18 column (Waters, Atlantis T3 Column, 4.6 mm × 50 mm, USA). The solution pH was measured by a pH meter (Leici, Shanghai). EPR (Bruker EMXPlus-10/12) spectra were recorded to analyze the generated reactive species using DMPO and TEMP as the spin-trapping agents. Details on the characterization instruments are provided in Text S1.

3. Results and discussion

3.1. *Catalytic performances of OS-X-AW samples*

It is reported that the pyrolysis temperature plays a key role in tuning the composition and surface chemistry of carbon-based materials, hereby affecting the catalytic performance (Chen et al., 2019). Therefore, the PMS activation efficiencies of OS-X-AW samples were compared in phenol degradation to optimize the pyrolysis temperature for OS. As illustrated in Fig. 1a, an adsorption-desorption equilibrium of phenol onto OS-X-AW was reached in 35 min and only ~5% phenol was removed by the adsorption process. Upon addition of PMS, phenol concentration was further reduced, suggesting the effectiveness of OS-based catalysts in PMS activation. Among six OS-X-AW/PMS systems, OS-550-AW/PMS and OS-600-AW/PMS exhibited the best degradation performance, i.e., a complete removal of phenol within 40 min, while the OS-600-AW slightly outperformed OS-550-AW. OS-650-AW/PMS system manifested a 100% removal efficiency within 80 min, higher than that of OS-400-AW/PMS (~30%), OS-700-AW/PMS (~30%) and OS-500-AW/PMS systems (~70%). As a result, 600 °C was found to be the optimal pyrolysis temperature for preparing OS-derived carbon-based catalysts and was adopted in the followed study. To understand the effect of temperature on the catalytic activity of OS-X-AW sample, thermogravimetric (TG) and differential thermogravimetric (DTG) analyses were conducted. As shown in Fig. 1b, the pyrolysis of OS could be roughly divided into three stages. The weight loss in stage I (30–200 °C) of 15% was mainly caused by the volatilization of moisture and release of volatile organic matter in the OS (Guo et al., 2010). The major weight loss of ~48% occurred at stage II (200–600 °C), which originated from the decomposition of heavy compounds into smaller distillable molecules and gases like CO, CO_2, CH_4 and H_2 (Pánek et al., 2014). A small weight loss of 7% at stage III (600–900 °C) was resulted from the secondary decomposition of OS-based char and other inorganic materials present in the sludge (Pánek et al., 2014; Huang et al., 2015; Thangalazhy-Gopakumar et al., 2015). Hence, incomplete pyrolysis of OS was induced at the low temperature (<600 °C) while the high temperature (>600 °C) possibly caused a decrease of active sites in the catalyst, which are not beneficial to the catalytic activity.

PMS and PDS are two primary oxidants used in PS-AOPs, while they possess different molecular structures, which may result in distinct activation efficiency over the same catalyst. Consequently, we compared the activation efficiencies of OS-600-AW for PMS and PDS via degrading phenol under the same experimental conditions. As shown in Fig. S1, a much lower phenol removal efficiency of 70% was attained by OS-600-AW/PDS system than that of OS-600-AW/PMS system (100%), suggesting the better catalytic activity of OS-600-AW towards PMS activation. This can be attributed to the asymmetric structure of PMS, which makes it easier to be decomposed than the symmetric PDS (Ike et al., 2018).

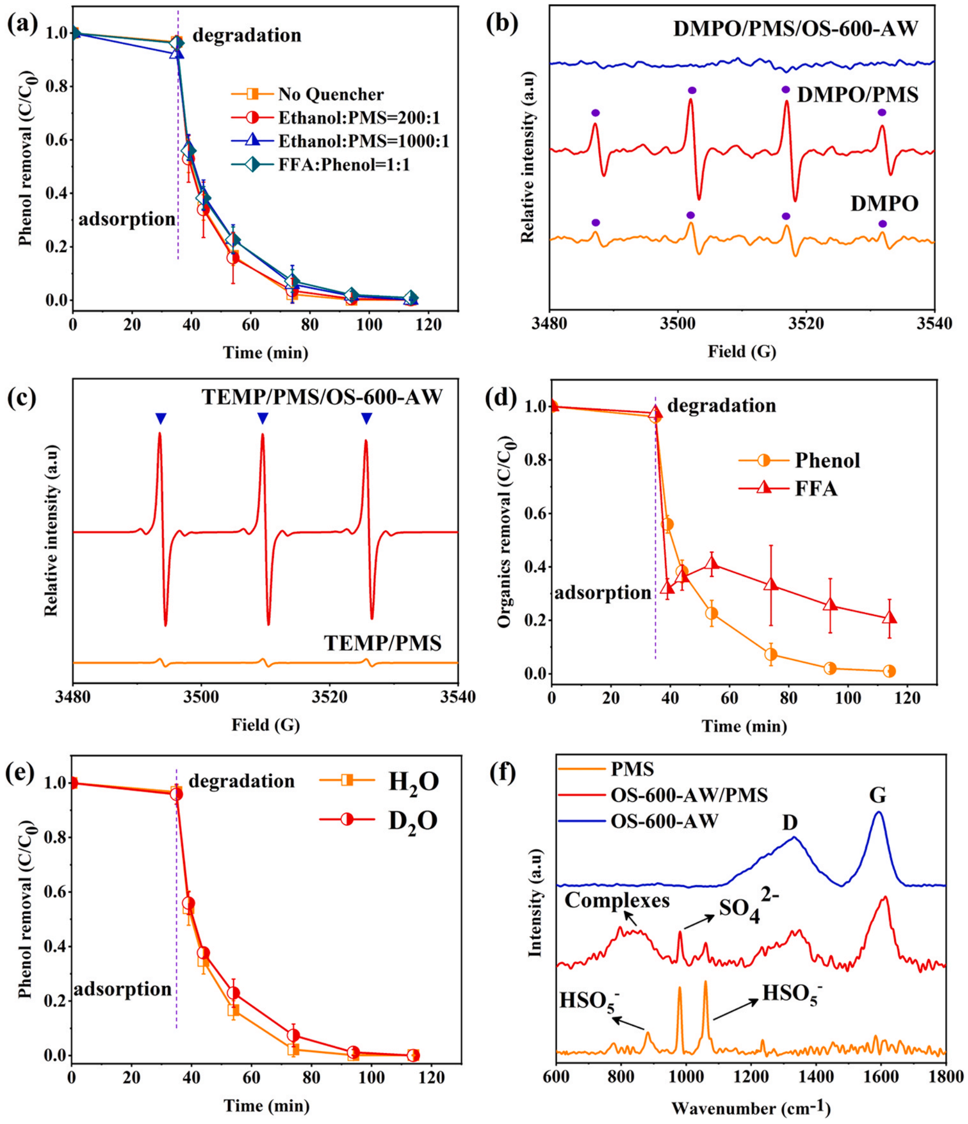

Fig. 2. (a) Removals of phenol in the presence of ethanol and FFA by OS-600-AW/PMS system; EPR spectra of OS-600-AW/PMS system using (b) DMPO and (c) TEMP as trapping agents (●: DMPO•-OH adducts; ▼: TEMP-$^1O_2$ adducts); (d) Simultaneous removal of FFA and phenol by OS-600-AW/PMS system; (e) Removal of phenol by OS-600-AW/PMS system in H_2O and D_2O solution; (f) Raman spectra of the PMS solution alone, OS-600-AW and OS-600-AW in the PMS solution. Conditions: $[catalyst] = 0.2\ g\ L^{-1}$, $[PMS]_0 = 0.925$ mM, $[DMPO]_0 = 110$ mM, $[TEMP]_0 = 10$ mM, $[phenol]_0 = 50\ mg\ L^{-1}$, $[FFA]_0 = 0.53$ mM, $[ethanol]_0 = 0.185$ M, 0.925 M.

3.2. Optimization of the OS-600-AW/PMS system

A suitable pH environment for phenol oxidation over OS-600-AW/PMS system was investigated. As shown in Fig. 1c, a degradation efficiency of ~100% was attained under a wide pH range of 2–10, suggesting the good tolerance of OS-600-AW/PMS system for pH. Notably, faster phenol oxidation was observed under an acidic environment (2–6) compared to the basic environment (8–10), and the fastest oxidation achieved at pH of 2. This phenomenon is explained by the variation of surface charge of the carbon-based catalyst. According to Fig. 1d, OS-600-AW has a pH_{zpc} value (the point of zero charge) of 3.4. Hence, the surface of OS-600-AW was positively charged at $pH < 3.4$, which enhanced the interaction between the catalyst and PMS molecules and thus the activation efficiency (Jung et al., 2016; Nie et al., 2019; Zheng et al., 2019).

Since sulfate ions are released from the persulfate activation process while the sulfate ions can corrode the sewage systems (Zhu et al., 2018), it is necessary to optimize the PMS dosage for pollutant abatement over OS-600-AW/PMS system for minimizing the potential environmental risk of the sulfate ions. Fig. S2 describes the phenol removal behavior by OS-600-AW/PMS system under a fixed catalyst concentration of $0.2\ g\ L^{-1}$ and various PMS dosages (0.04–5.55 mM). As shown, the removal efficiency increased from 10% to 80% with the PMS concentration from 0.04 to 0.49 mM, and a further rise of PMS concentration (0.93–5.55 mM) accelerated the oxidation rate. Interestingly, a good linear fitting ($R^2 = 0.997$) between the PMS concentration and phenol removal efficiency was observed (Fig. 1e) and a minimal [PMS/Phenol] molar ratio of 1.11 for complete removal of phenol was derived from the linear correlation.

The average oxidant utilization rate is defined as mol pollutant per mol oxidant per hour for phenol degradation by OS-600-AW/PMS system. This factor is also used as an index of the catalytic activity of persulfate activator (Sun et al., 2020). A value of 0.87 mol phenol per mol PMS per hour at a catalyst dosage of $0.2\ g\ L^{-1}$ was derived for OS-600-AW, which was much higher than those of other persulfate activators reported in literature (Table S2), implying the practicability of OS-derived catalyst for water remediation. Furthermore, TOC removal efficiency during the phenol degradation process in OS-600-AW/PMS system was measured. Around 80% phenol was mineralized into carbon dioxide and water within 80 min, revealing the good mineralization ability of OS-600-AW/PMS system.

Furthermore, the performances of OS-600-AW/PMS system for degrading other micropollutants including 2,4-dichlorobromobenzene, carbamazepine, and BPA were also investigated. As shown in Fig. 1f, an adsorption-desorption equilibrium of those micropollutants onto OS-600-AW was reached in 35 min and about 43%, 36%, and 31% organics were removed by the adsorption process for 2,4-dichlorobromobenzene, carbamazepine, and BPA, respectively. Upon PMS addition, the concentrations of the organic compounds were dramatically reduced, while PMS alone can barely oxidize the organics (Fig. S3), suggesting the effectiveness of OS-600-AW/PMS system for degrading diverse micropollutants. More specifically, 100% removal of 2,4-dichlorobromobenzene in 44 min, 100% removal of BPA in 59 min and 73% of carbamazepine in 79 min were attained.

3.3. Influences of anions on the phenol removal by OS-600-AW/PMS system

The ubiquitous inorganic anions in natural waters may react with persulfate or the generated ROS, interfering the abatement of organic pollutants by persulfate-based AOPs (Meng et al., 2020). In this work, the influences of Cl^-, HCO_3^- and CO_3^{2-} ions on phenol degradation performance of OS-600-AW/PMS system were studied. As shown in Fig. S4a, the presences of both 4 mM and 8 mM Cl^- had a slight promoting effect on phenol removal, possibly ascribing to that the excessive Cl^- can easily react with PMS to form $HOCl/Cl_2$ with strong oxidizing capacity (Li et al., 2021). However, presences of both CO_3^{2-} and HCO_3^- show a remarkable impact in the degradation performance of OS-600-AW/PMS system. Fig. S4b depicts that the phenol removal efficiency was decreased to 70% when 2 mM or 4 mM CO_3^{2-} was added into the OS-600-AW/PMS system, while only 80% or 60% phenol was removed with the addition of 2 mM or 6 mM respectively. These phenomena are explained by the reason that PMS can be activated by CO_3^{2-} and HCO_3^- (Duan et al., 2016), but the PMS activation efficiency by CO_3^{2-} or HCO_3^- is lower than OS-600-AW, resulting in a faster consumption of PMS and inhibited phenol degradation.

3.4. Identification of nonradical oxidation pathway based on electron-transfer mechanism

To discern the primary ROS in OS-600-AW/PMS system responsible for phenol oxidation, quenching experiments using ethanol for both $SO_4^{\bullet -}$ and •OH ($K_{SO_4^{\bullet -}} = 1 \times 10^7 M^{-1} S^{-1}, K_{HO^\bullet} = 1 \times 10^9 M^{-1} S^{-1}$) and FFA for $^1O_2$ ($K_{1_{O_2}} = 1.2 \times 10^8 M^{-1} S^{-1}$) were carried out (Chen et al., 2018; Sun et al., 2020). Fig. 2a illustrated that the presence of ethanol with a molar ratio of Ethanol:PMS = 200:1 barely inhibited the degradation of phenol in OS-600-AW/PMS system, and the excessive addition of ethanol (Ethanol:PMS = 1000:1) only slightly reduced the phenol oxidation rate. Meanwhile, the presence of FFA exerted a similar effect on phenol degradation as the presence of excessive ethanol (Ethanol: PMS = 1000:1), i.e., a marginal inhibitory effect. These results reveal that the organic pollutant elimination by OS-600-AW/PMS system was relied on neither free radicals nor $^1O_2$. Consequently, electron-transfer mechanism is proposed to be involved in the OS-600-AW/PMS system.

EPR technique was further employed to examine the ROS generated from PMS activation catalyzed by OS-600-AW. The EPR spectra (Fig. 2b) show that a weak signal of DMPO-•OH adducts was detected in solution with PMS alone (no catalyst), originating from the slight hydrolysis of PMS (Duan et al., 2018b). However, the signal vanished upon the addition of OS-600-AW catalyst. It is probably because that PMS was rapidly decomposed over the carbocatalyst and DMPO was oxidized by the ROS produced in the OS-600-AW/PMS system, leading to the no detection of DMPO-•OH adducts signal. This observation consolidated that free radicals were not produced by OS-600-AW/PMS system. However, a more prominent three-line signal of 2,2,6,6-tetramethylpiperidine-N-oxyl (TEMPO) in Fig. 2c, which is normally attributed to the formation of TEMP-$^1O_2$ adducts, was observed for the OS-600-AW/PMS system compared to the PMS alone system (Luo et al., 2019). This indicates the possible generation of $^1O_2$ from PMS activation catalyzed by OS-600-AW, contradicting to the FFA quenching test. Two reasons are likely to explain the inconsistence between FFA quenching test and EPR detection: (i) the strong TEMPO signal detected in OS-600-AW/PMS system is resulted from the oxidation of TEMP by the metastable reactive intermediate formed between PMS and catalyst rather than $^1O_2$ (Wang et al., 2019); (ii) $^1O_2$ was generated in OS-600-AW/PMS system but it was not responsible for the phenol oxidation.

To identify whether $^1O_2$ was generated in OS-600-AW/PMS system, simultaneous removal of FFA and phenol by OS-600-AW/PMS system was also tested. As depicted in Fig. 2d, both FFA and phenol were effectively degraded in the OS-600-AW/PMS system, while the degradation efficiency for FFA was lower than that of phenol. Because the reaction rate constant of $^1O_2$ with FFA is higher than that with phenol, the above results indicated that $^1O_2$ indeed existed in OS-600-AW/PMS system and it preferentially reacted with FFA, whereas phenol was oxidized via the electron-transfer mechanism.

Furthermore, phenol degradation in D_2O solution was also investigated in order to rule out the contribution of $^1O_2$. As known, the lifetime of $^1O_2$ in D_2O (20–32 μS) is much longer than that in H_2O (2 μS) (Luo et al., 2019). In this context, the oxidation of organics in D_2O can be significantly improved if $^1O_2$ dominates the reaction. However,

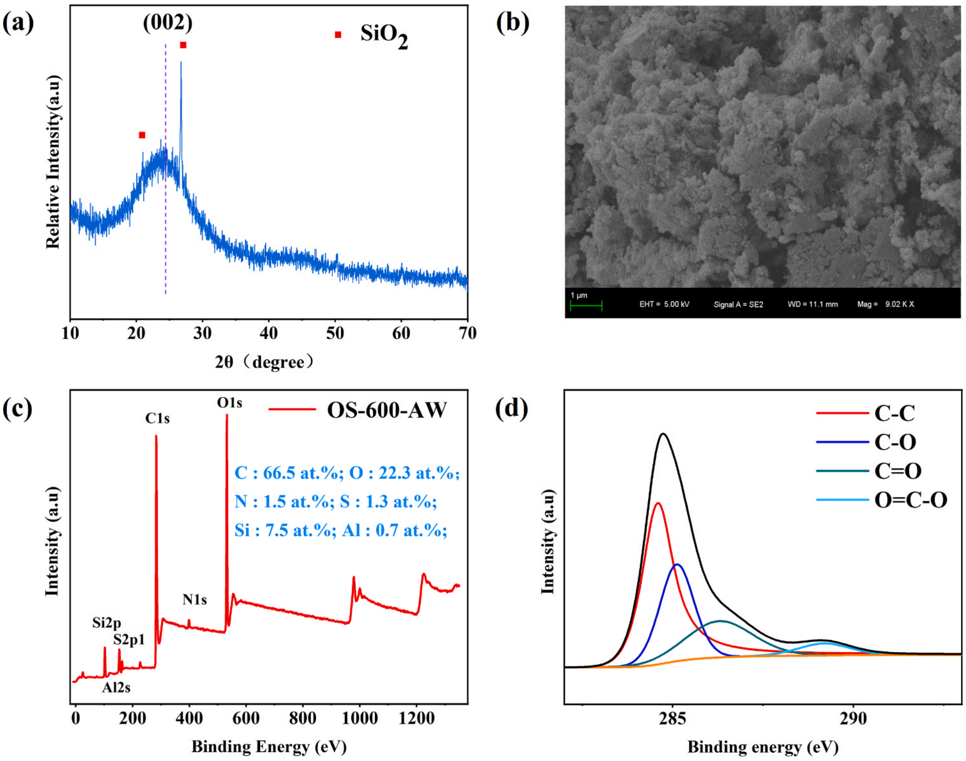

Fig. 3. (a) XRD pattern, (b) SEM image, (c) XPS full scan spectrum and (d) deconvoluted C1s XPS peak of OS-600-AW.

enhanced degradation performance in D_2O solution was not exhibited by the OS-600-AW/PMS system (Fig. 2e). Therefore, nonradical oxidation pathway via electron-transfer mechanism dominating in the OS-600-AW/PMS system was well proved. Additionally, the surface bonding reaction between catalyst and PMS was also supported by in situ Raman spectroscopy. According to Fig. 2f, prominent D peak at 1358 cm^{-1} and G peak at 1585 cm^{-1} are recorded in the Raman spectrum of OS-600-AW, attributing to the disordered carbon structures and in-plane stretching motion of sp^2 carbon atoms in the catalyst, respectively (Gangupomu et al., 2016). Two characteristic peaks at around 890 and 1050 cm^{-1} assignable to HSO_5^- and one at ~980 cm^{-1} corresponding to SO_4^{2-} were observed for pure PMS. However, after the interaction between PMS with OS-600-AW, the intensity of HSO_5^- peak of PMS at ~1050 cm^{-1} was diminished while the HSO_5^- peak at ~890 cm^{-1} was significantly broadened and shifted to 831 cm^{-1}. These phenomena suggested the decomposition of PMS by OS-600-AW and the formation of reactive complexes bonding to the surface active site of the catalyst (Zhang et al., 2013; Ding et al., 2013; Guan et al., 2017).

3.5. *Characterizations of catalysts*

A broad peak at 2θ of ~25° attributed to the (002) plane of graphitic carbon is observed in the XRD pattern of OS-600-AW (Fig. 3a), indicating the amorphous carbon structure (Wang et al., 2019). Meanwhile, two sharp peaks at 2θ of ~21° and ~27° are also present in the XRD pattern, which originate from SiO_2 particles in pristine OS (Li et al., 2017; Wang et al., 2017; Hu et al., 2019). The SEM image of OS-600-AW also illustrates that the carbon-based catalyst is composed of amorphous and irregular particles with different sizes (Fig. 3b). The SSA of OS-600-AW is measured to be 663.7 $m^2\ g^{-1}$, which is higher than those of maize straw-, peanut-, bamboo-, chestnut-, and sludge-derived biochars (Wu et al., 2019). The full-scan XPS survey shows that the surface of OS-600-AW is mainly consisted of C and O elements (Fig. 3c) (Luo et al., 2019). Meanwhile, small amount of Si and trace amount of N, S and Al are also contained in the carbon-based catalyst (Fig. 3c). It should be noted that SiO_2 and Al_2O_3 are inactive to PMS (Ike et al., 2018; Mian et al., 2019). Therefore, carbons in OS-600-AW catalyst intrinsically act as the catalytic centers for PMS activation. Additionally, the solid residue obtained from the combustion of OS-600-AW in air (e-OS-600-AW) was also found to be incapable of activating PMS to degrade phenol, further confirming the metal-free nature of the OS-600-AW catalyst (Fig. S5). The deconvoluted C1s XPS spectrum of OS-600-AW in Fig. 3d shows that the surface of the OS-600-AW catalyst is oxygen-enriched with different percentages of C-O (285.1 eV), C=O (286.2 eV), and O=C-O (289.2 eV) (Smith et al., 2016; Varga et al., 2017).

Interestingly, Fe and alkaline (e.g. Na, Mg, Ca) elements are detected on the surface of OS-600 sample through XPS survey, which originate from the metal ions in pristine OS derivation (Fig. S6), while the catalytic activity of OS-600 towards PMS activation was lower than that of OS-600-AW (Fig. S7). This phenomenal reveals the superiority of carbon-based catalyst to metal-based catalyst in PMS activation. However, the metal ions in OS were found to be responsible for the formation of active sites in OS-600-AW. As shown in Fig. S8, the OS(HCl)-600-AW catalyst prepared from the pre-rinsed OS precursor with HCl solution manifested a declined catalytic activity than OS-600-AW, as evidenced by the reduction of phenol removal efficiency to 50%. Hence, it is deduced that the metal ions in the OS probably play a role in the formation of active sites in OS-derived catalysts during the pyrolysis process.

3.6. *Determination of active sites in OS-600-AW*

The surface oxygenated groups especially C=O on carbocatalysts have been commonly suggested to play important roles in activating PMS via radical- or $^1O_2$-based oxidation pathway (Wang et al., 2016; Li et al., 2020). However, a recent study by Guo et al. proposed that C=O was the main active site in CNTs responsible for the electron-transfer mechanism, while $^1O_2$ was generated at CNTs defects based on the comparison of catalytic activity between pristine and modified CNTs for persulfate activation (Cheng et al., 2019). To verify whether C=O was also the primary catalytic site in OS-600-AW for activating PMS via electron-transfer mechanism, a series of chemical oxidation or reduction

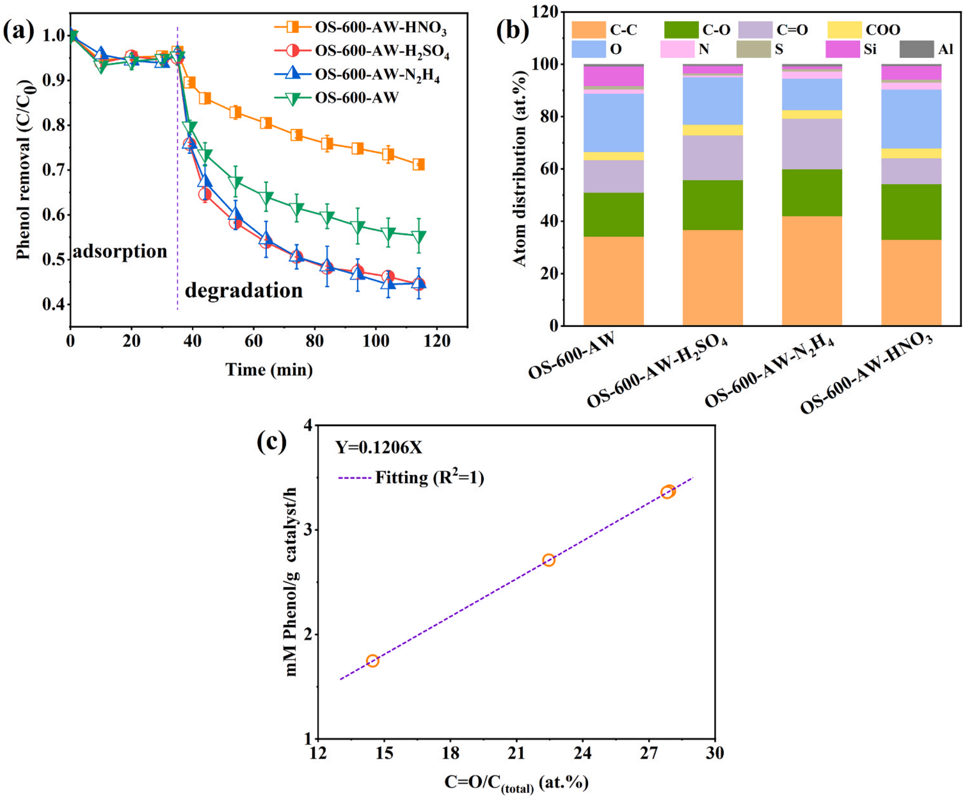

Fig. 4. (a) Catalytic performances of pristine OS-AW-600 and modified OS-AW-600 for activating PMS to remove phenol. Conditions: [catalyst] = 0.2 g L^{-1}, $[phenol]_0$ = 150 mg L^{-1}, $[PMS]_0$ = 0.925 mM; (b) Atomic distribution of OS-600-AW with chemical treatments; (c) Simulation of the catalytic activity of carbon-based catalyst versus C=O/$C_{(total)}$ (at%).

treatments were additionally conducted to modify the surface chemistry of the carbocatalyst. Fig. 4a shows that the phenol degradation performance with the reduced OS-600-AW (OS-600-AW-N_2H_4) or the OS-600-AW treated by H_2SO_4 (OS-600-AW-H_2SO_4) was remarkably enhanced compared to that of the unmodified carbocatalyst (Fan et al., 2010; Li et al., 2014; Huang et al., 2018). Oppositely, the catalytic activity of OS-600-AW was suppressed after the oxidation treatment with HNO_3 (OS-600-AW-HNO_3) because the phenol removal efficiency was decreased from 45% to 29%.

The C1s XPS spectra of those modified OS-derived carbocatalysts were further analyzed (Fig. S9) and the detailed compositions of different oxygenated groups are represented in Fig. 4b. The relative proportion of C=O (C=O/C_{total}) increased from 18.6 at% to 22.2 and 23.4 at% when OS-600-AW was treated with H_2SO_4 and N_2H_4, respectively, while it decreased to 14.5 at% with the HNO_3 treatment. Moreover, the proportion of C=O was found to have a good linear relationship (R^2 = 0.97) with the catalytic activity (Fig. 4c). As a result, C=O in the OS-derived carbon-based catalysts was likely to be the main active site for activating PMS to oxidize the organics.

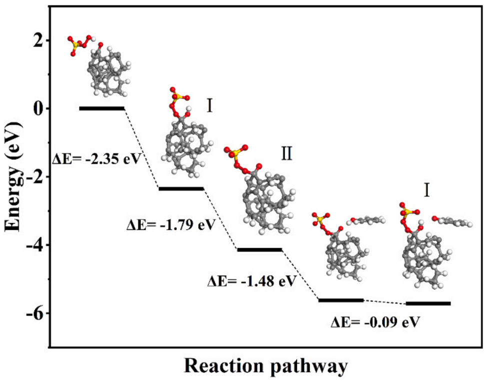

Fig. 5. Evolution of surface reactive complexes from the interaction between C=O in OS-600-AW and PMS molecule, oxidation of phenol by the formed reactive complexes and the corresponding reaction energies. Color codes: the white, gray, red and yellow are hydrogen, carbon, oxygen and sulfur atoms, respectively. (For interpretation of the references to colour in this figure, the reader is referred to the web version of this article.)

To gain insight into the interaction between C=O and PMS molecules during activation process and the evolution of the surface-bounded reactive complexes in the nonradical OS-600-AW/PMS system, we performed density functional theory (DFT) calculations. Relevant theoretical methodology is described in Text S2. Previously, we theoretically investigated the thermodynamic feasibility of the proposed reaction pathways for generating $^1O_2$ from the reactions of PMS over the C=O site in carbocatalyst (Meng et al., 2020). We discovered that the HSO_5^- ion in solution initially reacted with C=O in a biochar catalyst to form the intermediate (I) via an exothermic process. Then the intermediate (I) underwent dehydrogenation resulting in the generation of the intermediate (II), which was also an exothermic reaction. However, the further transformation of intermediate (II) into dioxirane was an endothermic process, which was usually regarded as the rate-determining step to produce $^1O_2$. These results cause us to wonder whether the intermediate (II) shows an oxidative capacity towards organic pollutant and it would preferentially react with the organics rather than being converted into dioxirane. To verify this hypothesis, we reconsidered the interaction between HSO_5^- and C=O in OS-600-AW to form reactive complexes and the redox reaction between the reactive complexes and phenol by employing DFT calculations. An amorphous carbon sphere is used to represent the OS-600-AW. As described in Fig. 5 and Eqs. (1)–(3), the first two reaction steps resemble to those in our previous work (Meng et al., 2020) and the intermediates (I) and (II) with similar structures were formed via exothermic processes. Then the possible reaction between intermediate (II) and phenol was computed. It was revealed that the phenol molecule could be easily adsorbed onto the intermediate (II) with an adsorption energy of −1.48 eV (exothermic). Subsequently, the intermediate (II) attracted one H atom in the -OH group of phenol to produce phenol anion and intermediate (I) (Eq. (3)) (Su et al., 2020), which was also an exothermic process releasing energy of 0.09 eV (Zhao et al., 2020). Notably, the initial total charges of the SO_5 moiety in intermediate (II) and phenol were −1.6538 e and −0.2038 e respectively, while a significant increase or reduction of the charges occurred after the H atom abstraction reaction between intermediate (II) and phenol. The total charges of the SO_5^- moiety in intermediate (I) and phenol anion were calculated to be −1.2675 e and −0.5300 e respectively, verifying the charge transfer from phenol to intermediate (II) (Fig. S10) via electron-transfer mechanism. Meanwhile, the reaction pathways for generating $^1O_2$ from the interaction between PMS and the C=O site in OS-600-AW was also calculated for comparison (Fig. S11). Apparently, the occurrence of reaction in Eq. (3) was more thermodynamically favorable than that of the transformation of dioxirane (intermediate (III) in Fig. S11), because the latter was endothermic with an energy of 0.29 eV. Hence, the above results suggested that the HSO_5^- ion tends to bond with the C=O active site in OS-600-AW to form intermediate (II) as the surface reactive complexes to oxidize phenol via a nonradial oxidation pathway(Su et al., 2020). Regarding the detection of $^1O_2$ in the OS-600-AW/PMS system, we deduced that other functionalities than C=O group in the carbocatalyst were primarily responsible for decomposing PMS to produce $^1O_2$, while the reaction steps between PMS and C=O group as shown in Fig. S11 probably made a small contribution to $^1O_2$ production. To conclude, by combining the experimental and computational results, the key role of C=O group in OS-600-AW for activating PMS to degrade phenol via an electron-transfer mechanism was well consolidated and the evolution processes of the surface reactive complexes were elucidated.

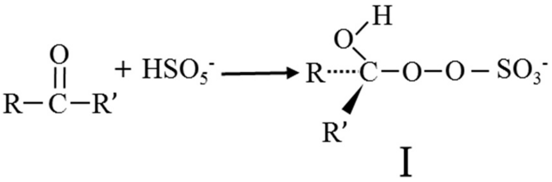

(1)

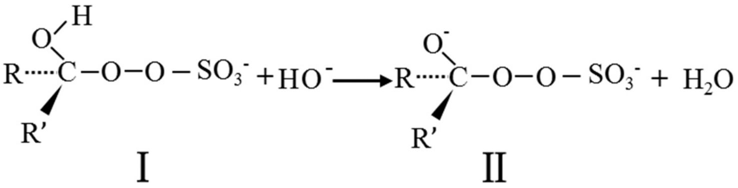

(2)

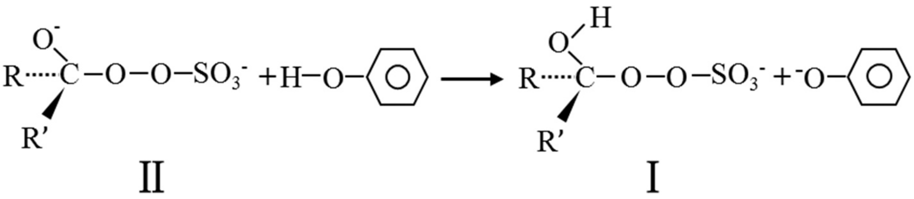

(3)

3.7. *Stability and regeneration of OS-600-AW catalyst*

The stability of OS-600-AW was also evaluated. As displayed in Fig. S12, OS-600-AW deactivated greatly because only a phenol degradation efficiency of 20% was attained after three runs. To understand the deactivation mechanism, the surface chemistry of OS-600-AW collected after the first run (reused) was examined by XPS. It was found that the C content in OS-600-AW was decreased from 66.57 at% (fresh) to 63.94 at% (reused) and the O content was increased from 22.31 at% (fresh) to 25.81 at% (reused) respectively. This indicated that the carbocatalyst was partially oxidized by PMS or ROS generated from PMS activation during the phenol degradation process. Additionally, the content of C=O in OS-600-AW was remarkably decreased from 22.46 at % (fresh) to 14.47 at% (reused) (Fig. S13), revealing that the active sites in carbocatalyst were consumed during the activation process. Because of the consumption of active sites and partial oxidation of OS-600-AW which deteriorates the electron transport ability of carbocatalyst, deactivation of carbocatalyst was induced.

Thermal treatment was reported to regenerate the deactivated active sites of carbon materials (Zhu et al., 2019). Consequently, the reused OS-600-AW were heated at 300 °C, 400 °C and 500 °C for 2 h in N_2 to recover their catalytic activity, respectively. As illustrated in Fig. S14, the degradation of phenol was restored to some extent after thermal treatment. Compared with the reused OS-600-AW, the degradation efficiencies of regenerate OS-600-AW heated at 300 °C, 400 °C and 500 °C increased by 27%, 32% and 36%, respectively. This implies that thermal treatment is a feasible method for the regeneration of reused carbonaceous materials (Jiang et al., 2018).

4. Conclusions

In this study, we show that carbon-based materials prepared by a facile one-pot pyrolysis treatment on OS can be employed as metal-free catalysts for PMS activation and oxidative degradation of micropollutants. The optimized OS-600-AW sample was demonstrated to manifest high catalytic activity for activating PMS to rapidly oxidize multiple organic pollutants. By optimizing the operation parameters, 50 ppm phenol could be completely degraded in 40 min by OS-600-AW/PMS system at the catalyst dosage of $0.2\ g\ L^{-1}$ and PMS dosage of 0.925 mM under a wide pH range of 2–10. Meanwhile, the involved mechanisms in the OS-600-AW/PMS system for degrading organic pollutants were investigated. It was discovered that $^1O_2$ and surface reactive complexes were both evolved in the OS-600-AW/PMS system but electron-transfer mechanism mainly accounted for the oxidation of pollutants. Moreover, C=O was identified as the main active site on OS-600-AW responsible for the nonradical PMS activation based on electron-transfer mechanism rather than singlet oxygenation mechanism. The findings in this study are of great significance for not only the proper disposal and reuse of OS wastes but also offering an advanced strategy for practical remediation of aqueous organic pollutants.

CRediT authorship contribution statement

Wenjie Liu: Investigation, Data curation, Formal analysis, Writing - original draft. **Chunyang Nie:** Co-supervising, Data curation, Writing - review & editing. **Wenlang Li:** DFT calculation, Co-Writing - original draft. **Zhimin Ao:** Conceptualization, Supervision, Funding acquisition, Validation, Writing - review & editing. **Shaobin Wang:** Supervision, Writing - review & editing. **Taicheng An:** Writing - review & editing, Supervision.

Declaration of Competing Interest

The authors declare that they have no known competing financial interests or personal relationships that could have appeared to influence the work reported in this paper.

Acknowledgements

This work was supported by the National Natural Science Foundation of China (NO. 21806024 and 21777033), China Postdoctoral Science Foundation (NO. 2017M622637), Science and Technology Planning Project of Guangdong Province (NO. 2017B020216003), Guangdong Natural Science Foundation (NO. 2020A1515011150) and the Innovation Team Project of Guangdong Provincial Department of Education (NO. 2017KCXTD012).

Appendix A. Supporting information

Supplementary data associated with this article can be found in the online version at doi:10.1016/j.jhazmat.2021.125552.

References

Ávila-Chávez, M.A., Eustaquio-Rincón, R., Reza, J., Trejo, A., 2007. Extraction of hydrocarbons from crude oil tank bottom sludges using supercritical ethane. Sep. Sci. Technol. 42, 2327–2345.

Brauer, H.-D., Eilers, B., Lange, A., 2002. Formation of singlet molecular oxygen by the Radziszewski reaction between acetonitrile and hydrogen peroxide in the absence and presence of ketones,. J. Chem. Soc. Perkin Trans. 2, 1288–1295.

Chen, X., Oh, W.-D., Lim, T.-T., 2018. Graphene- and CNTs-based carbocatalysts in persulfates activation: material design and catalytic mechanisms. Chem. Eng. J. 354, 941–976.

Chen, Y.D., Bai, S., Li, R., Su, G., Duan, X., Wang, S., Ren, N.Q., Ho, S.H., 2019. Magnetic biochar catalysts from anaerobic digested sludge: production, application and environment impact. Environ. Int. 126, 302–308.

Cheng, X., Guo, H., Zhang, Y., Liu, Y., Liu, H., Yang, Y., 2016. Oxidation of 2,4-dichlorophenol by non-radical mechanism using persulfate activated by Fe/S modified carbon nanotubes. J. Colloid Interface Sci. 469, 277–286.

Cheng, X., Guo, H., Zhang, Y., Korshin, G.V., Yang, B., 2019. Insights into the mechanism of nonradical reactions of persulfate activated by carbon nanotubes: activation performance and structure-function relationship. Water Res. 157, 406–414.

Ding, Y., Zhu, L., Wang, N., Tang, H., 2013. Sulfate radicals induced degradation of tetrabromobisphenol A with nanoscaled magnetic CuFe2O4 as a heterogeneous catalyst of peroxymonosulfate. Appl. Catal. B Environ. 129, 153–162.

Duan, X., Ao, Z., Sun, H., Indrawirawan, S., Wang, Y., Kang, J., Liang, F., Zhu, Z.H., Wang, S., 2015. Nitrogen-doped graphene for generation and evolution of reactive radicals by metal-free catalysis. ACS Appl. Mater. Interfaces 7, 4169–4178.

Duan, X., Su, C., Zhou, L., Sun, H., Suvorova, A., Odedairo, T., Zhu, Z., Shao, Z., Wang, S., 2016. Surface controlled generation of reactive radicals from persulfate by carbocatalysis on nanodiamonds. Appl. Catal. B Environ. 194, 7–15.

Duan, X., Ao, Z., Zhou, L., Sun, H., Wang, G., Wang, S., 2016. Occurrence of radical and nonradical pathways from carbocatalysts for aqueous and nonaqueous catalytic oxidation. Appl. Catal. B Environ. 188, 98–105.

Duan, X., Ao, Z., Zhang, H., Saunders, M., Sun, H., Shao, Z., Wang, S., 2018a. Nanodiamonds in sp(2)/sp(3) configuration for radical to nonradical oxidation: core-shell layer dependence. Appl. Catal. B Environ. 222, 176–181.

Duan, X., Sun, H., Shao, Z., Wang, S., 2018b. Nonradical reactions in environmental remediation processes: uncertainty and challenges. Appl. Catal. B Environ. 224, 973–982.

Duan, X., Sun, H., Wang, S., 2018c. Metal-free carbocatalysis in advanced oxidation reactions. Acc. Chem. Res. 51, 678–687.

Duan, X., Tian, W., Zhang, H., Sun, H., Ao, Z., Shao, Z., Wang, S., 2019. sp2/sp3 framework from diamond nanocrystals: a key bridge of carbonaceous structure to carbocatalysis. ACS Catal. 9, 7494–7519.

Fan, Y., Wang, B., Yuan, S., Wu, X., Chen, J., Wang, L., 2010. Adsorptive removal of chloramphenicol from wastewater by NaOH modified bamboo charcoal. Bioresour. Technol. 101, 7661–7664.

Fernandez-Luqueno, F., Valenzuela-Encinas, C., Marsch, R., Martinez-Suarez, C., Vazquez-Nunez, E., Dendooven, L., 2011. Microbial communities to mitigate contamination of PAHs in soil–possibilities and challenges: a review. Environ. Sci. Pollut. Res. 18, 12–30.

Ferrarese, E., Andreottola, G., Oprea, I.A., 2008. Remediation of PAH-contaminated sediments by chemical oxidation. J. Hazard. Mater. 152, 128–139.

Fonts, I., Gea, G., Azuara, M., Ábrego, J., Arauzo, J., 2012. Sewage sludge pyrolysis for liquid production: a review. Renew. Sustain. Energy Rev. 16, 2781–2805.

Gangupomu, R.H., Sattler, M.L., Ramirez, D., 2016. Comparative study of carbon nanotubes and granular activated carbon: physicochemical properties and adsorption capacities. J. Hazard. Mater. 302, 362–374.

Ghanbari, F., Moradi, M., 2017. Application of peroxymonosulfate and its activation methods for degradation of environmental organic pollutants: review. Chem. Eng. J. 310, 41–62.

Guan, C., Jiang, J., Luo, C., Pang, S., Jiang, C., Ma, J., Jin, Y., Li, J., 2016. Transformation of iodide by carbon nanotube activated peroxydisulfate and formation of iodoorganic compounds in the presence of natural organic matter. Environ. Sci. Technol. 51, 479–487.

Guan, C., Jiang, J., Pang, S., Luo, C., Ma, J., Zhou, Y., Yang, Y., 2017. Oxidation kinetics of bromophenols by nonradical activation of peroxydisulfate in the presence of carbon nanotube and formation of brominated polymeric products. Environ. Sci. Technol. 51, 10718–10728.

Guo, X., Wang, S., Guo, Z., Liu, Q., Luo, Z., Cen, K., 2010. Pyrolysis characteristics of bio-oil fractions separated by molecular distillation. Appl. Energy 87, 2892–2898.

Hu, G., Li, J., Zeng, G., 2013. Recent development in the treatment of oily sludge from petroleum industry: a review. J. Hazard. Mater. 261, 470–490.

Hu, W., Xie, Y., Lu, S., Li, P., Xie, T., Zhang, Y., Wang, Y., 2019. One-step synthesis of nitrogen-doped sludge carbon as a bifunctional material for the adsorption and catalytic oxidation of organic pollutants. Sci. Total Environ. 680, 51–60.

Huang, B.-C., Jiang, J., Huang, G.-X., Yu, H.-Q., 2018. Sludge biochar-based catalysts for improved pollutant degradation by activating peroxymonosulfate. J. Mater. Chem. A 6, 8978–8985.

Huang, Q., Wang, J., Qiu, K., Pan, Z., Wang, S., Chi, Y., Yan, J., 2015. Catalytic pyrolysis of petroleum sludge for production of hydrogen-enriched syngas. Int. J. Hydrog. Energy 40, 16077–16085.

Ike, I.A., Linden, K.G., Orbell, J.D., Duke, M., 2018. Critical review of the science and sustainability of persulphate advanced oxidation processes. Chem. Eng. J. 338, 651–669.

Indrawirawan, S., Sun, H., Duan, X., Wang, S., 2015. Nanocarbons in different structural dimensions (0–3D) for phenol adsorption and metal-free catalytic oxidation. Appl. Catal. B Environ. 179, 352–362.

Jiang, L., Zhang, Y., Zhou, M., Liang, L., Li, K., 2018. Oxidation of Rhodamine B by persulfate activated with porous carbon aerogel through a non-radical mechanism. J. Hazard. Mater. 358, 53–61.

Jung, K.W., Choi, B.H., Hwang, M.J., Jeong, T.U., Ahn, K.H., 2016. Fabrication of granular activated carbons derived from spent coffee grounds by entrapment in calcium alginate beads for adsorption of acid orange 7 and methylene blue. Bioresour. Technol. 219, 185–195.

Kriipsalu, M., Marques, M., Nammari, D.R., Hogland, W., 2007. Bio-treatment of oily sludge: the contribution of amendment material to the content of target contaminants, and the biodegradation dynamics. J. Hazard. Mater. 148, 616–622.

Lai, C.K., Chen, G., Lo, M.C., 2004. Salinity effect on freeze/thaw conditioning of activated sludge with and without chemical addition. Sep. Purif. Technol. 34, 155–164.

Lee, H., Lee, H.-J., Jeong, J., Lee, J., Park, N.-B., Lee, C., 2015. Activation of persulfates by carbon nanotubes: oxidation of organic compounds by nonradical mechanism. Chem. Eng. J. 266, 28–33.

Lei, X., You, M., Pan, F., Liu, M., Yang, P., Xia, D., Li, Q., Wang, Y., Fu, J., 2019. CuFe2O4@GO nanocomposite as an effective and recoverable catalyst of peroxymonosulfate activation for degradation of aqueous dye pollutants. Chin. Chem. Lett. 30, 2216–2220.

Li, J., Li, Y., Xiong, Z., Yao, G., Lai, B., 2019. The electrochemical advanced oxidation processes coupling of oxidants for organic pollutants degradation: a mini-review. Chin. Chem. Lett. 30, 2139–2146.

Li, J., Li, M., Sun, H., Ao, Z., Wang, S., Liu, S., 2020. Understanding of the oxidation behavior of benzyl alcohol by peroxymonosulfate via carbon nanotubes activation. ACS Catal. 10, 3516–3525.

Li, K., Ma, S., Xu, S., Fu, H., Li, Z., Li, Y., Liu, S., Du, J., 2021. The mechanism changes during bisphenol A degradation in three iron functionalized biochar/peroxymonosulfate systems: the crucial roles of iron contents and graphitized carbon layers. J. Hazard. Mater. 404, 124145.

Li, Y., Shao, J., Wang, X., Deng, Y., Yang, H., Chen, H., 2014. Characterization of modified biochars derived from bamboo pyrolysis and their utilization for target component (Furfural) adsorption. Energy Fuels 28, 5119–5127.

Li, Y., Yang, Z., Zhang, H., Tong, X., Feng, J., 2017. Fabrication of sewage sludge-derived magnetic nanocomposites as heterogeneous catalyst for persulfate activation of Orange G degradation. Colloids Surf. A Physicochem. Eng. Asp. 529, 856–863.

Luo, K., Yang, Q., Pang, Y., Wang, D., Li, X., Lei, M., Huang, Q., 2019. Unveiling the mechanism of biochar-activated hydrogen peroxide on the degradation of ciprofloxacin. Chem. Eng. J. 374, 520–530.

Luo, R., Li, M., Wang, C., Zhang, M., Nasir Khan, M.A., Sun, X., Shen, J., Han, W., Wang, L., Li, J., 2019. Singlet oxygen-dominated non-radical oxidation process for efficient degradation of bisphenol A under high salinity condition. Water Res. 148, 416–424.

Ma, M., Chen, L., Zhao, J., Liu, W., Ji, H., 2019. Efficient activation of peroxymonosulfate by hollow cobalt hydroxide for degradation of ibuprofen and theoretical study. Chin. Chem. Lett. 30, 2191–2195.

Ma, Z., Gao, N., Xie, L., Li, A., 2014. Study of the fast pyrolysis of oilfield sludge with solid heat carrier in a rotary kiln for pyrolytic oil production. J. Anal. Appl. Pyrolysis 105, 183–190.

Malviya, R., Chaudhary, R., 2006. Factors affecting hazardous waste solidification/stabilization: a review. J. Hazard. Mater. 137, 267–276.

Meng, H., Nie, C., Li, W., Duan, X., Lai, B., Ao, Z., Wang, S., An, T., 2020. Insight into the effect of lignocellulosic biomass source on the performance of biochar as persulfate activator for aqueous organic pollutants remediation: epicarp and mesocarp of citrus peels as examples. J. Hazard. Mater. 399, 123043.

Meng, X., Cao, Q., Jin, Le, Zhang, X., Gong, S., Li, P., 2016. Carbon electrode materials for supercapacitors obtained by co-carbonization of coal-tar pitch and sawdust. J. Mater. Sci. 52, 760–769.

Mian, M.M., Liu, G., Fu, B., Song, Y., 2019. Facile synthesis of sludge-derived MnOx-N-biochar as an efficient catalyst for peroxymonosulfate activation. Appl. Catal. B Environ. 255, 117765.

Nazem, M.A., Tavakoli, O., 2017. Bio-oil production from refinery oily sludge using hydrothermal liquefaction technology. J. Supercrit. Fluids 127, 33–40.

Nie, C., Dai, Z., Meng, H., Duan, X., Qin, Y., Zhou, Y., Ao, Z., Wang, S., An, T., 2019. Peroxydisulfate activation by positively polarized carbocatalyst for enhanced removal of aqueous organic pollutants. Water Res. 166, 115043.

Nie, C., Dai, Z., Liu, W., Duan, X., Wang, C., Lai, B., Ao, Z., Wang, S., An, T., 2020. Criteria of active sites in nonradical persulfate activation process from integrated experimental and theoretical investigations: boron–nitrogen-co-doped nanocarbon-mediated peroxydisulfate activation as an example. Environ. Sci. Nano 7, 1899–1911.

Nii, S., Kikumoto, S., Tokuyama, H., 2009. Quantitative approach to ultrasonic emulsion separation. Ultrason Sonochem. 16, 145–149.

Pánek, P., Kostura, B., Čepeláková, I., Koutník, I., Tomšej, T., 2014. Pyrolysis of oil sludge with calcium-containing additive. J. Anal. Appl. Pyrolysis 108, 274–283.

Paranhos Gazineu, M.H., de Araujo, A.A., Brandao, Y.B., Hazin, C.A., de, O.G.J.M., 2005. Radioactivity concentration in liquid and solid phases of scale and sludge generated in the petroleum industry. J. Environ. Radioact. 81, 47–54.

Ren, W., Xiong, L., Nie, G., Zhang, H., Duan, X., Wang, S., 2019. Insights into the electron-transfer regime of peroxydisulfate activation on carbon nanotubes: the role of oxygen functional groups. Environ. Sci. Technol. 54, 1267–1275.

Smith, M., Scudiero, L., Espinal, J., McEwen, J.-S., Garcia-Perez, M., 2016. Improving the deconvolution and interpretation of XPS spectra from chars by ab initio calculations. Carbon 110, 155–171.

Su, H., Wei, Y., Qu, X., Yu, C., Li, Q., Alvarez, P.J.J., Long, M., 2020. Mechanistic inference on the reaction kinetics of phenols and anilines in carbon nanotubes-activated peroxydisulfate systems: pp-LFERs and QSARs analyses. Chem. Eng. J. 385, 123923.

Sun, C., Chen, T., Huang, Q., Zhan, M., Li, X., Yan, J., 2020. Activation of persulfate by CO_2-activated biochar for improved phenolic pollutant degradation: performance and mechanism. Chem. Eng. J. 380, 122519.

Sun, H., Kwan, C., Suvorova, A., Ang, H.M., Tadé, M.O., Wang, S., 2014. Catalytic oxidation of organic pollutants on pristine and surface nitrogen-modified carbon nanotubes with sulfate radicals. Appl. Catal. B Environ. 154–155, 134–141.

Sun, H., Peng, X., Zhang, S., Liu, S., Xiong, Y., Tian, S., Fang, J., 2017. Activation of peroxymonosulfate by nitrogen-functionalized sludge carbon for efficient degradation of organic pollutants in water. Bioresour. Technol. 241, 244–251.

Thangalazhy-Gopakumar, S., Al-Nadheri, W.M.A., Jegarajan, D., Sahu, J.N., Mubarak, N.M., Nizamuddin, S., 2015. Utilization of palm oil sludge through pyrolysis for bio-oil and bio-char production. Bioresour. Technol. 178, 65–69.

Varga, M., Izak, T., Vretenar, V., Kozak, H., Holovsky, J., Artemenko, A., Hulman, M., Skakalova, V., Lee, D.S., Kromka, A., 2017. Diamond/carbon nanotube composites: Raman, FTIR and XPS spectroscopic studies. Carbon 111, 54–61.

Wang, C., Kang, J., Sun, H., Ang, H.M., Tadé, M.O., Wang, S., 2016. One-pot synthesis of N-doped graphene for metal-free advanced oxidation processes. Carbon 102, 279–287.

Wang, H., Guo, W., Liu, B., Wu, Q., Luo, H., Zhao, Q., Si, Q., Sseguya, F., Ren, N., 2019. Edge-nitrogenated biochar for efficient peroxydisulfate activation: An electron transfer mechanism. Water Res. 160, 405–414.

Wang, J., Liu, T.-L., Huang, Q.-X., Ma, Z.-Y., Chi, Y., Yan, J.-H., 2017. Production and characterization of high quality activated carbon from oily sludge. Fuel Process. Technol. 162, 13–19.

Wang, X., Gu, L., Zhou, P., Zhu, N., Li, C., Tao, H., Wen, H., Zhang, D., 2017. Pyrolytic temperature dependent conversion of sewage sludge to carbon catalyst and their performance in persulfate degradation of 2-Naphthol. Chem. Eng. J. 324, 203–215.

Wang, Y., Ao, Z., Sun, H., Duan, X., Wang, S., 2016. Activation of peroxymonosulfate by carbonaceous oxygen groups: experimental and density functional theory calculations. Appl. Catal. B Environ. 198, 295–302.

Wu, C., Liu, X., Wu, X., Dong, F., Xu, J., Zheng, Y., 2019. Sorption, degradation and bioavailability of oxyfluorfen in biochar-amended soils. Sci. Total Environ. 658, 87–94.

Yuan, X., Guan, R., Wu, Z., Jiang, L., Li, Y., Chen, X., Zeng, G., 2018. Effective treatment of oily scum via catalytic wet persulfate oxidation process activated by Fe(2). J. Environ. Manag. 217, 411–415.

Yun, E.T., Lee, J.H., Kim, J., Park, H.D., Lee, J., 2018. Identifying the nonradical mechanism in the peroxymonosulfate activation process: singlet oxygenation versus mediated electron transfer. Environ. Sci. Technol. 52, 7032–7042.

Yun, E.-T., Lee, J.H., Kim, J., Park, H.-D., Lee, J., 2018. Identifying the nonradical mechanism in the peroxymonosulfate activation process: singlet oxygenation versus mediated electron transfer. Environ. Sci. Technol. 52, 7032–7042.

Zhang, H., Ji, Q., Lai, L., Yao, G., Lai, B., 2019. Degradation of p-nitrophenol (PNP) in aqueous solution by mFe/Cu-air-PS system. Chin. Chem. Lett. 30, 1129–1132.

Zhang, T., Zhu, H., Croue, J.P., 2013. Production of sulfate radical from peroxymonosulfate induced by a magnetically separable CuFe2O4 spinel in water: efficiency, stability, and mechanism. Environ. Sci. Technol. 47, 2784–2791.

Zhao, C., Zhang, Z., Liu, Y., Shang, N., Wang, H.-J., Wang, C., Gao, Y., 2020. Palladium nanoparticles anchored on sustainable chitin for phenol hydrogenation to cyclohexanone. ACS Sustain. Chem. Eng. 8, 12304–12312.

Zheng, W., Xiao, X., Chen, B., 2019. A nonradical reaction-dominated phenol degradation with peroxydisulfate catalyzed by nitrogen-doped graphene. Sci. Total Environ. 667, 287–296.

Zhou, Y., Jiang, J., Gao, Y., Ma, J., Pang, S.Y., Li, J., Lu, X.T., Yuan, L.P., 2015. Activation of peroxymonosulfate by benzoquinone: a novel nonradical oxidation process. Environ. Sci. Technol. 49, 12941–12950.

Zhou, Y., Jiang, J., Gao, Y., Pang, S.Y., Yang, Y., Ma, J., Gu, J., Li, J., Wang, Z., Wang, L.H., Yuan, L.P., Yang, Y., 2017. Activation of peroxymonosulfate by phenols: Important role of quinone intermediates and involvement of singlet oxygen. Water Res. 125, 209–218.

Zhu, K., Wang, X., Chen, D., Ren, W., Lin, H., Zhang, H., 2019. Wood-based biochar as an excellent activator of peroxydisulfate for Acid Orange 7 decolorization. Chemosphere 231, 32–40.

Zhu, S., Huang, X., Ma, F., Wang, L., Duan, X., Wang, S., 2018. Catalytic removal of aqueous contaminants on N-doped graphitic biochars: inherent roles of adsorption and nonradical mechanisms. Environ. Sci. Technol. 52, 8649–8658.

Zubaidy, E.A.H., Abouelnasr, D.M., 2010. Fuel recovery from waste oily sludge using solvent extraction. Process Saf. Environ. Prot. 88, 318–326.